

# Magnetic anisotropies of quantum dots doped with magnetic ions

Karel Výborný,<sup>1,2</sup> J. E. Han,<sup>1</sup> Rafał Oszwaldowski,<sup>1</sup> Igor Žutić,<sup>1</sup> and A. G. Petukhov<sup>3</sup>

<sup>1</sup>*Department of Physics, University at Buffalo–SUNY, Buffalo, New York 14260, USA*

<sup>2</sup>*Institute of Physics, ASCR, v. v. i., Cukrovarnická 10, CZ-16253 Praha 6, Czech Republic*

<sup>3</sup>*South Dakota School of Mines and Technology, Rapid City, South Dakota 57701, USA*

(Received 4 November 2011; revised manuscript received 14 February 2012; published 12 April 2012)

Magnetic anisotropies in quantum dots (QDs) doped with magnetic ions are discussed in terms of two frameworks: anisotropic  $g$  factors and magnetocrystalline anisotropy energy. It is shown that even a simple model of zinc-blende  $p$ -doped QDs displays a rich diagram of magnetic anisotropies in the QD parameter space. Tuning the confinement allows us to control magnetic easy axes in QDs in ways not available for the better-studied bulk dilute magnetic semiconductors.

DOI: [10.1103/PhysRevB.85.155312](https://doi.org/10.1103/PhysRevB.85.155312)

PACS number(s): 73.21.La, 75.75.-c, 75.30.Gw, 75.50.Pp

## I. INTRODUCTION

Once the origin of magnetic ordering in a specific material is understood, it is often important to determine its magnetic anisotropy (MA) and hard and easy magnetic axes in particular. A shift of focus toward MA has already occurred for the studies of bulk dilute magnetic semiconductors (DMS),<sup>1,2</sup> but not yet fully for magnetic quantum dots (QDs) where it could play a certain role, for example, in the context of transport phenomena,<sup>3</sup> the formation of robust magnetic polarons,<sup>4-7</sup> control of magnetic ordering,<sup>8-12</sup> nonvolatile memory,<sup>13</sup> and quantum bits.<sup>14</sup>

In epilayers of (Ga,Mn)As, a prototypical DMS, the magnetocrystalline anisotropy energy (MAE) has been found to be a significant and often dominant source of MA (Refs. 15–17) caused by a strong spin-orbit (SO) coupling. It turns out that the easy-axis direction depends on hole concentration, magnetic doping level, as well as on other parameters. For example, when (Ga,Mn)As was used as a spin injector, the effects of strain (by altering the choice of a substrate) were responsible for changing the in-plane to out-plane easy axis.<sup>18</sup> While the strong SO coupling<sup>19</sup> is also present in  $p$ -type QD of zinc-blende materials doped with Mn, its effect on magnetic anisotropies will be significantly modified by the confinement. The energy levels in such “nanomagnets,”<sup>20-23</sup> where the Mn-Mn interaction is mediated by carriers, depend on the magnetization direction  $\mathbf{e}_M = (n_x, n_y, n_z)$ . It is often assumed that the interaction of magnetic moments with holes in quantum wells (QWs) or, equivalently, in flat QDs is effectively Ising-type.<sup>14,24</sup> Here, we quantify this assumption and explore MA using two frameworks: (i) an effective two-level Hamiltonian with a carrier  $g$  tensor,<sup>25</sup> which is widely employed also in theory of electron spin resonance, and (ii) MAE, which is commonly used to study bulk magnets.

While previous studies focused on specific nonmagnetic QDs (Ref. 26) and properties sensitive to system details (such as precise position of magnetic ions<sup>22,27</sup>), we explore more generic magnetic QD models, which can also serve as a starting point for more elaborate work. We consider a Hamiltonian comprising nonmagnetic and magnetic parts

$$\hat{H} = \hat{H}_{\text{QD}} + \hat{H}_{\text{ex}}. \quad (1)$$

The former encodes both QD confinement and SO interaction, which is a prerequisite for magnetic anisotropies, and the latter

expresses the kinetic-exchange coupling between holes and localized magnetic moments. For transparency, we disregard the magnetostatic shape anisotropy<sup>28</sup> and assume that the QD contains a fixed number of carriers. We mostly focus on the case of a single hole; realistically, such a system can be a II-VI colloidal<sup>5</sup> or epitaxial<sup>6</sup> QD with a photoinduced carrier. Magnetic moments of the Mn atoms are taken to be perfectly ordered (collinear) and are treated at a mean-field level. The magnetic easy axis is then the direction  $\mathbf{e}_M$  for which the zero-temperature free energy  $F(\mathbf{e}_M)$  is minimized.

In this article, we take two different points of view on  $F(\mathbf{e}_M)$ . On one hand, we discuss the lowest terms of  $F(\mathbf{e}_M)$  expanded in powers of the direction cosines of magnetization ( $n_x^2 + n_y^2 + n_z^2 = 1$ ), inspired by the standard “bulk MAE phenomenology” and pay special attention to the case of perfectly cubic QDs,  $F(\mathbf{e}_M) = F_0(\mathbf{e}_M)$ . The anisotropies in  $F_0$  stem purely from the crystalline zinc-blende lattice. On the other hand,  $F(\mathbf{e}_M)$  acquires additional terms in systems with less symmetric confinement. We therefore discuss the anisotropic  $g$  factors as a useful framework to handle such systems, e.g., cuboid QDs (orthogonal parallelepiped; extremal cases are a cube and an infinitely thin slab, i.e., a QW) and show how the expansion

$$F(\mathbf{e}_M) = F_0(\mathbf{e}_M) + AF_1(\mathbf{e}_M) + A^2F_2(\mathbf{e}_M) + \dots \quad (2)$$

can be constructed using powers of  $A$  which reflect the anisotropy in  $g$  factors. We begin by discussing this latter topic in Sec. II [quantity  $A$  is defined by Eq. (8) at the end of Sec. II A], then proceed to the phenomenologic (symmetry-based) expansions of  $F_0$  in Sec. III and conclude that section with calculations of  $F_1$  in situations that are beyond the applicability of the  $g$ -factor framework.

## II. EFFECTIVE TWO-LEVEL HAMILTONIAN

Since  $\hat{H}_{\text{QD}}$  is invariant upon time reversal, its spectrum consists of Kramers doublets.<sup>29</sup> To study the ground-state energy in the presence of magnetic moments, we examine how these doublets are split by  $\hat{H}_{\text{ex}}(\mathbf{e}_M)$ , where  $\mathbf{e}_M$  is treated as an external parameter (related to classical magnetization; single-Mn doped QDs where the Mn magnetic moment behaves quantum mechanically<sup>30</sup> require different treatment), and represent them by an effective two-level Hamiltonian of Eq. (6). We consider two example systems: a simple four-level

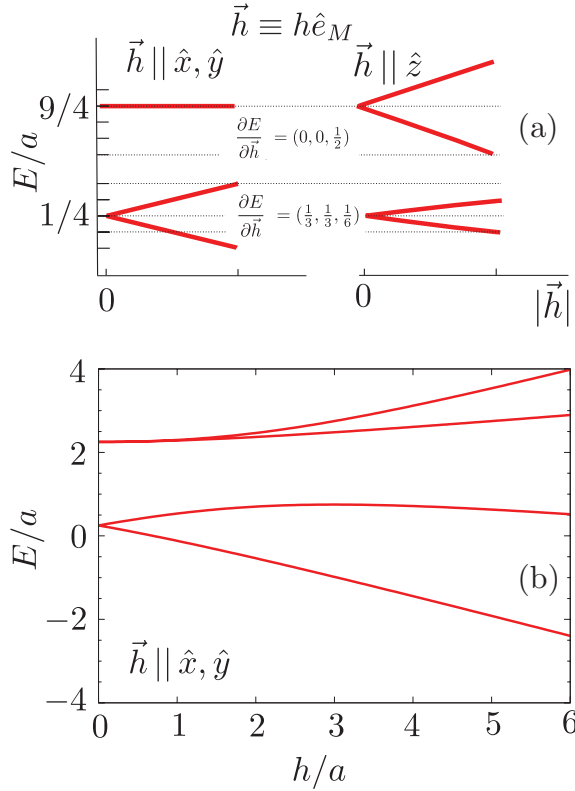


FIG. 1. (Color online) Splitting of levels  $E(h)$  in a flat QD described by Eq. (3). (a) For the particular Kramers doublet,  $E(h)$  depends on  $\mathbf{e}_M$  and the  $g$  factors (by convention non-negative) are  $\partial E/\partial \vec{h} = (g_x, g_y, g_z)$ . (b) Beyond the linear regime in  $h/a$ ,  $\partial E/\partial(hn_x)$  will be different for the upper and lower levels of the split doublet, it will depend on  $h$  and may even change sign, indicating that the  $\hat{H}_{\text{eff}}$  of Eq. (6) based on parameters  $g_{x,y,z}$  fails.

one where completely analytical treatment is possible, and a more realistic envelope-function-based model of a cuboid QD.

#### A. Four-level model

Related to the Kohn-Luttinger Hamiltonian of a QW,<sup>23,31</sup> the arguably simplest nontrivial model describing anisotropy of a flat QD is

$$\hat{H}_1 = a\hat{J}_z^2 + \frac{1}{3}h\mathbf{e}_M \cdot \hat{\mathbf{J}} \quad (3)$$

representing hole levels in a zinc-blende structure, the confinement anisotropy and exchange splitting of which are parametrized by  $a$  and  $h$ , respectively (the term  $a\hat{J}_z^2$  implies that the strongest confinement is along the  $z$  direction and this term also encodes information about the SO coupling).  $\hat{J}_{x,y,z}$  are  $4 \times 4$  spin- $\frac{3}{2}$  matrices. In terms of Eq. (1), we now choose  $\hat{H} = \hat{H}_1$  and the first (second) term in Eq. (3) plays the role of  $\hat{H}_{\text{QD}}$  ( $\hat{H}_{\text{ex}}$ ). Anisotropic behavior of eigenvalues of  $\hat{H}_1$ , to linear order in  $h/a$ , is illustrated in Fig. 1(a). It can be extracted from the exact eigenvalues

$$E_{\text{HH}}^{\pm}(h) = \frac{5}{4}a \pm \frac{1}{6}h + \sqrt{a^2 + \frac{1}{9}h^2 \mp \frac{1}{3}ah}, \quad (4)$$

$$E_{\text{LH}}^{\pm}(h) = \frac{5}{4}a \pm \frac{1}{6}h - \sqrt{a^2 + \frac{1}{9}h^2 \mp \frac{1}{3}ah} \quad (5)$$

in the case  $n_x = 1$  (or  $n_y = 1$ ), shown in Fig. 1(b), which clearly differ from the case  $n_z = 1$  where the eigenvalues are strictly linear functions of  $h$  ( $E_{\text{HH}}^{\pm} = 9a/4 \pm h/2$  and  $E_{\text{LH}}^{\pm} = a/4 \pm h/6$ ); subscripts refer to the  $E_{\text{HH}}^{\pm}(0) = 9a/4$  [heavy hole (HH)] and  $E_{\text{LH}}^{\pm}(0) = a/4$  [light hole (LH)] doublets, respectively. In the limit of weak exchange  $h/a \ll 1$ , splitting of each of the Kramers doublets is symmetric and it can be characterized by three parameters  $|\partial E/\partial(hn_p)|$ ,  $p = x, y, z$ , for  $h \rightarrow 0$  as depicted in Fig. 1(a). These parameters can be plausibly called, by analogy with the Zeeman effect, the anisotropic  $g$  factors  $g_p$ . From Eqs. (4) and (5), we straightforwardly obtain  $(g_x, g_y, g_z) = (0, 0, 1/2)$  and  $(1/3, 1/3, 1/6)$  for the HH and LH doublets of the Hamiltonian  $\hat{H}_1$ , respectively. This result is known from the context of QWs.<sup>31,32</sup> We emphasize that these  $g$  factors of the model specified by Eq. (3) are independent of the parameters  $a, h$  (except for the requirement  $h \ll a$ , which represents the  $h \rightarrow 0$  limit).

If we focus on one particular Kramers doublet, it is straightforward to show that  $\hat{H}_1$  projects to

$$\hat{H}_{\text{eff}} = h[n_x g_x \hat{\tau}_x + n_y g_y \hat{\tau}_y + n_z g_z \hat{\tau}_z] \quad (6)$$

for a suitably chosen basis  $|K_1\rangle, |K_2\rangle$  of the doublet. Here,  $\hat{\tau}_i$  are Pauli matrices and we have mapped two eigenstates of the original Hamiltonian  $\hat{H}_{\text{QD}}$  on a pseudospin  $|\vec{\tau}| = 1/2$  doublet  $|+\rangle, |-\rangle$ , where  $\hat{\tau}_z|\pm\rangle = \pm|\pm\rangle$ . For  $\hat{H} = \hat{H}_1$ , the eigenstates are only four dimensional (spanned by the  $|J_z = 3/2\rangle, |J_z = -1/2\rangle, |J_z = 1/2\rangle, |J_z = -3/2\rangle$  basis). We present another example of  $\hat{H}$  in Sec. II B where advantage of the projection becomes more apparent. The choice of basis  $|+\rangle, |-\rangle$  is crucial to obtain  $\hat{H}_{\text{eff}}$  in the simple form (6); considering the HH doublet,  $|+\rangle = |J_z = 3/2\rangle, |-\rangle = |J_z = -3/2\rangle$  leads to Eq. (6), while for other basis choices the mapping  $\hat{H}_{\text{ex}} = (h/3)\mathbf{e}_M \cdot \hat{\mathbf{J}} \mapsto \hat{H}_{\text{eff}} = h\mathbf{e}_M \cdot \mathbf{g} \cdot \hat{\tau}$  may lead<sup>31</sup> to the nonsymmetric tensor  $g = g_{ij}$ ,  $i, j \in \{x, y, z\}$ . In general, if the mapping is to produce  $g_{ij} = \text{diag}(g_x, g_y, g_z)$ , the “suitable choice of the basis  $|K_1\rangle, |K_2\rangle$ ” where  $|K_1\rangle \mapsto |+\rangle$  is such that  $\langle K_1|\hat{J}_{x,y}|K_1\rangle = 0, \langle K_1|\hat{J}_z|K_1\rangle \geq 0$  (and  $|K_2\rangle$  is the time-reversed image of  $|K_1\rangle$ , which is mapped to  $|-\rangle$ ).

Let us now consider a general system described by Eq. (1). Assuming that the downfolding of  $\hat{H}$  into  $\hat{H}_{\text{eff}}$  is possible for given  $|K_1\rangle, |K_2\rangle$  (this assumption is discussed in Appendix A), the anisotropic  $g$  factors can readily be determined as  $\partial E/\partial h$  for the particular Kramers doublet level  $E$ . This is equivalent to perturbatively evaluating the effect of  $\hat{H}_{\text{ex}}$  on two degenerate levels to the first order of  $h$  as follows: (i) specify the Kramers doublet of interest, and find any basis  $|K_1\rangle, |K_2\rangle$  of this doublet, (ii) extract the operators  $\hat{t}_{x,y,z}$  from  $\hat{H}_{\text{ex}}$  by taking  $\hat{t}_p = \partial \hat{H}_{\text{ex}}/\partial(n_p h)$  (for example,  $\hat{t}_x = \hat{J}_x/3$  for  $\hat{H}_{\text{ex}}$  appearing in  $\hat{H}_1$ ), (iii) evaluate their matrices

$$\tilde{t}_{x,y,z} = \begin{pmatrix} \langle K_1|\hat{t}_{x,y,z}|K_1\rangle & \langle K_1|\hat{t}_{x,y,z}|K_2\rangle \\ \langle K_2|\hat{t}_{x,y,z}|K_1\rangle & \langle K_2|\hat{t}_{x,y,z}|K_2\rangle \end{pmatrix} \quad (7)$$

in the two-dimensional space spanned by  $|K_1\rangle, |K_2\rangle$ , and (iv) the non-negative eigenvalue of  $\tilde{t}_p$  equals  $g_p$  ( $p = x, y, z$ ). We emphasize that while  $g_p$  depends on system parameters in  $\hat{H}_{\text{QD}}$  and  $\hat{H}_{\text{ex}}$ , it also depends on which Kramers doublet we choose. Higher doublets become relevant for QDs containing higher (odd) number of holes, for example.

The effective Hamiltonian in Eq. (6) can be used for various purposes, e.g., for studies of fluctuations of magnetization in magnetic QDs,<sup>33</sup> spin-selective tunneling through nonmagnetic QDs,<sup>34</sup> or excitons in single-Mn-doped QDs.<sup>35</sup> If the magnetic easy axis is of interest, the  $g$  factors immediately provide the answer:  $F(\mathbf{e}_M)$  based on Eq. (6) is minimized for  $\mathbf{e}_M$  in the direction of the largest  $g_p$  [e.g., for the HH doublet in Fig. 1(a), it is  $n_z = 1$  because  $g_z > g_x, g_y$ ]. If the full form of  $F(\mathbf{e}_M)$  is needed (e.g. for ferromagnetic resonance<sup>2</sup>), it can be straightforwardly obtained by diagonalizing the  $2 \times 2$  matrix of  $\hat{H}_{\text{eff}}$ . Assuming  $g_x = g_y$ , the (modulus of the) eigenvalue can be expanded in terms of parameters  $A$  and  $k$  as derived in Appendix B. It is meaningful to call

$$A = (g_z^2 - g_x^2)/(g_z^2 + g_x^2) \quad (8)$$

the asymmetry parameter since it vanishes in a perfectly cubic QD ( $g_x = g_y = g_z$ ) and it is with respect to this parameter that we can identify

$$AF_1(\mathbf{e}_M) = -Akn_z^2, \quad (9)$$

$$A^2F_2(\mathbf{e}_M) = +\frac{1}{8}A^2k(2n_z^2 - 1)^2 \quad (10)$$

in Eq. (2) to linear order of  $k \propto h$ .

### B. A cuboid quantum-dot model

With this general scheme at hand, we take one step in the hierarchy of models toward a more realistic description of magnetic QDs. We consider a zinc-blende structure  $p$ -doped semiconductor shaped into a cuboid of size  $L_x \times L_y \times L_z$  such as can be described by the four-band Kohn-Luttinger (KL) Hamiltonian.<sup>23</sup> Also in this system,  $\hat{H} = \hat{H}_2$  is a sum of  $\hat{H}_{\text{ex}}$  and  $\hat{H}_{\text{QD}}$ , but this time  $\hat{H}_{\text{QD}}$  comprises of blocks  $\langle m_x m_y m_z | \hat{H}_{\text{KL}} | m'_x m'_y m'_z \rangle$  with

$$\hat{H}_{\text{KL}} = \frac{\hbar^2}{2m_0} \left\{ \left( \gamma_1 + \frac{5}{2}\gamma_2 \right) p^2 - 2\gamma_2 [\hat{J}_x^2 \hat{p}_x^2 + \hat{J}_y^2 \hat{p}_y^2 + \hat{J}_z^2 \hat{p}_z^2] - 2\gamma_3 [(\hat{J}_x \hat{J}_y + \hat{J}_y \hat{J}_x) \hat{p}_x \hat{p}_y + \text{c.p.}] \right\}. \quad (11)$$

Here,  $|m_x m_y m_z\rangle$  denotes the basis of envelope functions,  $\gamma_{1,2,3}$  the Luttinger parameters,  $m_0$  the electron vacuum mass,  $\hat{p}_{x,y,z}$  the momentum operators, and c.p. denotes the cyclic permutation (see Appendix C for details). The envelope function is conveniently developed into harmonic functions with  $m_p - 1$  nodes in the  $p = x, y, z$  direction:

$$\langle \vec{r} | m_x m_y m_z \rangle = N \sin \frac{m_x \pi x}{\lambda_x L} \sin \frac{m_y \pi y}{\lambda_y L} \sin \frac{m_z \pi z}{L}. \quad (12)$$

We have introduced the dimensionless aspect ratios  $\lambda_{x,y} = L_{x,y}/L$  and the normalization factor  $N$ . Our system can be viewed as an infinitely deep potential well with  $V(x, y, z) = 0$  for  $0 < x < L_x$ ,  $0 < y < L_y$ ,  $0 < z < L_z \equiv L$ , and infinite otherwise.

For fixed material parameters (Luttinger parameters in ratios  $\gamma_2/\gamma_1$ ,  $\gamma_3/\gamma_2$ ) and QD shape ( $\lambda_x, \lambda_y$ ), all matrix elements of all blocks  $\langle m_x m_y m_z | \hat{H}_{\text{KL}} | m'_x m'_y m'_z \rangle$  scale as  $1/L^2$ . The spectrum, consisting of Kramers doublets which occasionally combine into larger multiplets, is specified by a sequence of

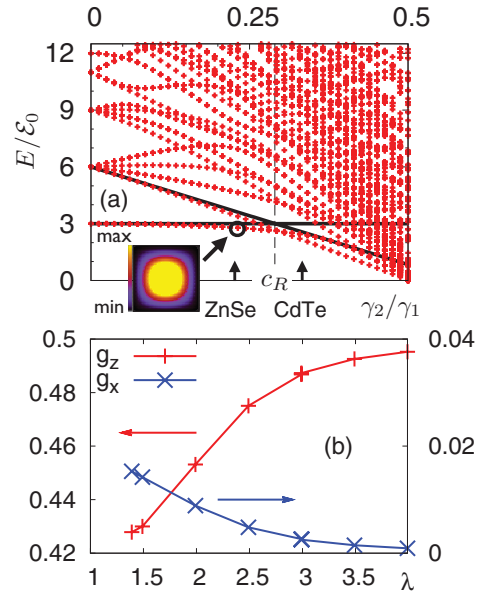


FIG. 2. (Color online) (a) Levels in a cubic dot (with  $\gamma_3 = \gamma_2$ ) in units of  $\mathcal{E}_0$  defined by Eq. (13). Solid lines indicate the analytic result obtained when mixing between remote levels is disregarded. Note that their crossing (which we use to discern the weak and strong HH/LH splitting materials, dashed line) is very close to the actual crossing when level mixing is taken into account. Values representing ZnSe ( $\bar{\gamma}_2/\gamma_1 \approx 0.23$ ) and CdTe ( $\bar{\gamma}_2/\gamma_1 \approx 0.33$ ) QDs are indicated. Inset: squared wave-function modulus of the ZnSe QD ground state in the  $z = L/2$  section. (b) Dependence of the  $g$  factors associated with the ground-state Kramers doublet in a CdTe QD on its shape ( $\lambda_x = \lambda_y \equiv \lambda$ ).

dimensionless numbers  $E/\mathcal{E}_0$ , where

$$\mathcal{E}_0 = \hbar^2 \pi^2 \gamma_1 / (2m_0 L^2). \quad (13)$$

For a cubic QD [ $\lambda_x = \lambda_y = 1$ ; see Fig. 2(a)], the  $s$ -like state shown in the inset of Fig. 2(a) forms a quadruplet, and depending on the value of  $\gamma_2/\gamma_1$  (and to a somewhat lesser extent also of  $\gamma_3/\gamma_2$ ), this state competes with the next doublet for having the lowest energy. The critical value (see Appendix C)

$$c_R = (2 + 128/9\pi^2)^{-1} \approx 0.29 \quad (14)$$

can be taken to distinguish materials with small ( $\gamma_2/\gamma_1 < c_R$ , ground-state quadruplet) and large ( $\gamma_2/\gamma_1 > c_R$ , ground-state doublet) splitting between light and heavy holes in the bulk; these can be ZnSe and CdTe, respectively, and their values of  $\bar{\gamma}_2/\gamma_1$  based on approximating  $\gamma_2$  and  $\gamma_3$  by their average  $\bar{\gamma}_2 = (\gamma_2 + \gamma_3)/2$  are indicated in Fig. 2(a). By numerical diagonalization, we have determined the lowest 7 Kramers doublets in slightly deformed QDs ( $\lambda_x = \lambda_y \equiv \lambda = 1.01$ ) in these materials ( $\gamma_1 = 4.8$ ,  $\gamma_2 = 0.67$ , and  $\gamma_3 = 1.58$  for ZnSe and  $\gamma_1 = 4.1$ ,  $\gamma_2 = 1.1$ , and  $\gamma_3 = 1.6$  for CdTe),<sup>36</sup> and executed the procedures (i)–(iv) above to obtain the  $g$  factors which are listed in the Table I ( $g_x = g_y$  due to  $\lambda_x = \lambda_y$ ). To avoid confusion, we remark that in (i),  $|K_1\rangle, |K_2\rangle$  are vectors of dimension 864 in the basis  $|m_x m_y m_z\rangle \otimes |J_z\rangle$  (see the discussion of cutoff in Appendix C) and in (ii),  $\hat{t}_x = (1/3)\hat{J}_x \otimes \mathbb{1}_{xyz}$ , where  $\mathbb{1}_{xyz}$  is the identity operator in the space of the envelope functions given by Eq. (12). Evaluation and diagonalization of the

TABLE I. Energies and  $g$  factors in slightly deformed QDs ( $\lambda = 1.01$ ) for the lowest 7 Kramers doublets for ZnSe and CdTe, where  $\mathcal{E}_0 \approx 28$  and 24 meV, respectively, for  $L = 8$  nm.

CdTe			ZnSe		
$E$ [meV]	$g_x = g_y$	$g_z$	$E$ [meV]	$g_x = g_y$	$g_z$
49.9	0.166	0.164	71.7	0.012	0.464
52.8	0.027	0.418	71.9	0.305	0.171
53.0	0.269	0.176	92.1	0.167	0.160
78.5	0.162	0.169	126.1	0.274	0.237
84.1	0.010	0.129	129.6	0.076	0.069
84.4	0.064	0.004	130.0	0.082	0.045
85.6	0.203	0.279	141.0	0.205	0.212

$2 \times 2$  matrices in Eq. (7) requested in (iii) and (iv) is performed numerically. The possibility to map the action of  $\hat{H}_{\text{ex}} = (h/3)\mathbf{e}_M \cdot \hat{\mathbf{J}} \otimes \mathbb{1}_{xyz}$  on the Kramers doublets  $|K_1\rangle$ ,  $|K_2\rangle$  implied by  $\hat{H}_{\text{QD}}$  of a cuboid  $p$ -doped QD is discussed in Appendix A.

The slight deformation of the QD makes the quadruplet split into two doublets (with energies 71.7 and 71.9 meV for ZnSe), the  $g$  factors of which approach  $(0, 0, 1/2)$  and  $(1/3, 1/3, 1/6)$ . A similar situation occurs for the doublet pair with energies 52.8 and 53.0 meV for CdTe. The actual ground state in this material is a doublet of different orbital character than the quadruplet (we stress that this is due to the confinement, see Appendix C); it evolves from the  $E = 6\mathcal{E}_0$  level of  $\gamma_2/\gamma_1 = 0$  as shown by the solid line in Fig. 2(a) and its  $g$  factors are isotropic,  $(1/6, 1/6, 1/6)$  in the limit  $\lambda \rightarrow 1$ . However, this doublet remains the ground state only in rather symmetric QDs ( $\lambda \lesssim 1.25$  in CdTe) and for more strongly deformed QDs, the lower doublet of the  $E = 3\mathcal{E}_0$  (at  $\gamma_2/\gamma_1 = 0$ ) quadruplet becomes the ground state just as it is the case for ZnSe for arbitrarily small deformations  $\lambda > 1$ . In Fig. 2(b), we show how the  $g$  factors of the CdTe QD ground state depend on  $\lambda$  beyond the mentioned value  $\approx 1.25$ . These results, including the  $g$  factors, are independent of the QD size  $L$ , except for the energies which scale as  $1/L^2$  as mentioned above.

From Fig. 2, one may conclude that the Ising-type Hamiltonian is often an excellent approximation ( $g_x = g_y = 0$ , as others assume<sup>14,24,33–35</sup>) for the lowest Kramers doublet. To be more specific, we now discuss materials with small and large HH/LH splitting separately. For  $\gamma_2/\gamma_1 < c_R$ , the out-of-plane  $g$  factor ( $g_z$ ) overwhelmingly exceeds the in-plane one ( $g_x = g_y$ ) even for minute deformation of the QD; this can be seen from the numeric ZnSe data in Fig. 2. We find  $g_z = 0.464$  and  $g_x = g_y = 0.012$  for  $\lambda - 1$  as small as 0.01. For CdTe, which represents the other class ( $\gamma_2/\gamma_1 > c_R$ ), we find similar values ( $g_z = 0.418$ ) for the *second* Kramers doublet, while the lowest doublet remains rather isotropic ( $g_x = g_y = 0.166$  and  $g_z = 0.164$ ). As we make the QD deformation larger, these two doublets cross, so that the ground-state doublet is Ising type, while the second lowest doublet remains more isotropic. As mentioned above, this crossing occurs for  $\lambda \approx 1.25$  in CdTe, and data in Fig. 2(b) are only shown for  $\lambda > 1.25$ .

We now elaborate on the properties of the low-energy sector of  $\hat{H}_2$  (at  $h = 0$ ). Coupling between blocks of different  $|m_x m_y m_z\rangle$  vanishes when  $\gamma_3/\gamma_1, \gamma_2/\gamma_1 \rightarrow 0$ , and Eq. (3)

becomes in this limit the exact effective Hamiltonian of the lowest four levels ( $m_p = 1$  for all  $p = x, y, z$ ). They form a quadruplet for  $\lambda = 1$ , which splits into two doublets upon deformation of the QD; we can see it by writing

$$(111|\hat{H}_{\text{KL}}|111) = 3\mathcal{E}_0 \left[ \mathbb{1}_4 f(\lambda) - \hat{J}_z^2 (1 - \lambda^{-2}) \frac{2}{3} \frac{\gamma_2}{\gamma_1} \right], \quad (15)$$

where  $\mathbb{1}_4$  is a unit  $4 \times 4$  matrix and  $f(\lambda)$  is a certain function with  $\lim_{\lambda \rightarrow 1} f(\lambda) = 1$ . The lower doublet of this  $4 \times 4$  effective Hamiltonian has  $g_z = 1/2$  (when  $\lambda > 1$  and  $\gamma_2 > 0$ ) and therefore the values of  $g_z$  deviating from 0.5 (appearing in Fig. 2) occur only due to admixtures from higher-orbital ( $m_p > 1$ ) states of LH character. Indeed, going from ZnSe to CdTe, the mixing becomes stronger and  $g_z$  of the HH-like level drops from 0.464 to 0.418 ( $\lambda = 1.01$ , numerical data in Table I). While Eq. (3) may remain the effective Hamiltonian of the two doublets originating from  $|m_x m_y m_z\rangle = |111\rangle$  even for  $\gamma_2/\gamma_1 > c_R$  (CdTe levels of 52.8 and 53.0 meV in Fig. 2), for  $\lambda$  close to 1, there is the more isotropic doublet on the stage (49.9 meV in Fig. 2). Nevertheless, if  $\lambda$  is sufficiently large, the  $\hat{J}_z^2$  term in Eq. (11) will eventually dominate, it will suppress all mixing between HH and LH states, and the lowest doublet will again approach  $(g_x, g_y, g_z) = (0, 0, 0.5)$  as it is shown in Fig. 2(b).

### III. MAGNETOCRYSTALLINE ANISOTROPY ENERGY

In analogy to the bulk systems, even cubic QDs retain anisotropies. However, these cannot be described within the previous framework: for instance,  $g_x, g_y, g_z$  are all equal to  $1/6$  in the cubic CdTe QD ground state, hence  $A = 0$  in Eq. (8). One could replace  $g_{ij}$  by a higher-rank tensor to capture these effects, but MAE formalism of bulk magnets seems more customary and informative. Unlike the  $g$  factors, MAE analysis does not invoke the concept of Kramers doublets. The zero-temperature free energy  $F(\mathbf{e}_M)$  of a magnetic QD with a single hole is now simply the lowest eigenvalue of Eq. (1) and it can be expanded in powers of  $n_j$ . The lowest terms compatible with cubic symmetry are<sup>39</sup>

$$F_0 = K_c(n_x^4 + n_y^4 + n_z^4) + 27K_{c2}n_x^2n_y^2n_z^2. \quad (16)$$

For data calculated by numerically diagonalizing  $\hat{H} = \hat{H}_2$  (model described in Sec. II B), it turns out that Eq. (16) suffices to obtain good fits; for instance, the lower solid line in Fig. 3(a) corresponds to  $K_c = 0.83$  meV and  $K_{c2} = 0.075$  meV with easy axis along  $[111]$ . There, we have chosen Cd<sub>1-x</sub>Mn<sub>x</sub>Te as the material,  $L = 16$  nm, and  $h = 50$  meV, which corresponds to  $h = J_{pd}N_{\text{Mn}}S_{\text{Mn}}$  with  $x \approx 2.3\%$  (we take<sup>36</sup>  $|J_{pd}| = 60$  meV nm<sup>3</sup>,  $S_{\text{Mn}} = 5/2$  and  $N_{\text{Mn}} = 4x/a_l^2$  with CdTe lattice constant  $a_l = 0.648$  nm). Results in Fig. 3 are again subject to scaling, similar to the nonmagnetic spectra in Fig. 2(a). When the material parameters (specifically,  $\gamma_2/\gamma_1$  and  $\gamma_3/\gamma_2$ ) are fixed, the spectrum of  $\hat{H}_2$ , expressed in the units of  $\mathcal{E}_0$ , depends on a single dimensionless parameter

$$\check{Z} = h/\mathcal{E}_0 \equiv 2m_0hL^2/(\gamma_1\pi^2\hbar^2). \quad (17)$$

This scaling relates the spectra of, e.g., cubic dots of different sizes and Mn contents (if their respective values of  $\check{Z}$  are equal). Data in Fig. 3 therefore apply both to  $x = 2.3\%$  at  $L = 16$  nm (if left as they are) and  $x = 9.2\%$  at  $L = 8$  nm (if scaled

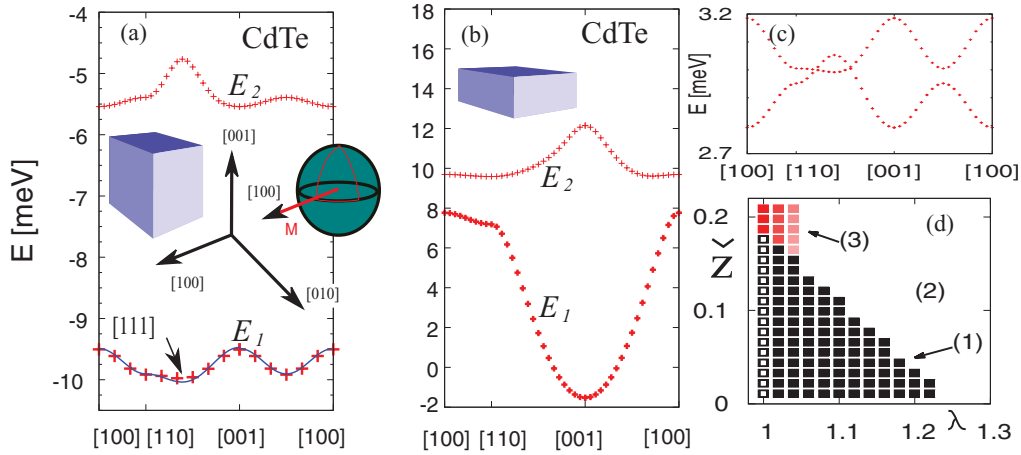


FIG. 3. (Color online) Magnetocrystalline energy as a function of magnetization direction ( $E_1$ ); the data labeled  $E_2$  are explained in the text. CdTe QD with 2.3% Mn (a)  $16 \times 16 \times 16 \text{ nm}^3$ , (b)  $16 \times 16 \times 8 \text{ nm}^3$ . (c) Fictitious material with parameters described in the text; note that the sign of  $K_c$  implied by Eq. (16) has changed compared to (a) and (b). (d) Color-coded easy-axis positions for CdTe QDs as a function of aspect ratio ( $\lambda$ ) and effective exchange splitting  $\tilde{Z}$ . Black squares (1) indicate easy plane perpendicular to the  $z$  direction, hollow squares denote an isotropic magnet; white region (2) corresponds to easy axis [001]; red squares (3) denote systems with [111] easy axis, which gradually shifts toward [001] with increasing  $\lambda$ . This plot is universal as far as  $L$  is concerned.

by a factor of 4). It turns out that the  $g$ -factor analysis presented in the previous section is meaningful for  $\tilde{Z} \lesssim 0.1$ , while now we have stepped out of this limit. When the exchange field  $h$  becomes stronger, levels cross and cease to depend linearly on  $h$  as required by Eq. (6); for  $\hat{H} = \hat{H}_1$ , this is illustrated in Fig. 1(b). This limit was determined for CdTe cubic QDs, but it will typically not be too different for other materials and/or aspect ratios  $\lambda$  unless accidental (quasi)degeneracies occur at  $\tilde{Z} = 0$ .

MAE shown in Fig. 3 describe systems well beyond this limit of small  $\tilde{Z}$  (linear regime). We first focus on a perfectly cubic CdTe QD where there are no anisotropies in the linear regime. As already mentioned, the lowest energy hole state in Fig. 3(a) exhibits a [111] easy axis with  $K_c = 0.83 \text{ meV}$  at  $L = 16 \text{ nm}$  and  $h = 50 \text{ meV}$ , i.e.,  $\tilde{Z} \approx 2.8$  (this corresponds to a realistic  $x \approx 2.3\%$  Mn doping). In bulk DMSs, [111] would be an unusual magnetic easy-axis direction<sup>15</sup> and we surmise that the reason for this is that, for instance in (Ga,Mn)As grown on a GaAs substrate, there is a sizable compressive strain which prefers either parallel or perpendicular orientation of  $\mathbf{e}_M$  with respect to the growth axis.

We note that in a QD containing two holes (closed-shell system<sup>11</sup>), the anisotropies will also be present and they will

be different from the single-hole case. Free energy, taken as a sum  $F_0(\mathbf{e}_M) = E_1 + E_2$  of the lowest two single-hole states [shown e.g. in Fig. 3(a)], is not a constant independent of  $\mathbf{e}_M$  as one could naively expect. This intuition reflects  $\hat{H}_{\text{eff}}$  in Eq. (6) where the two hole states have opposite spin (hence their energies add up to zero). Once we leave the linear regime ( $\tilde{Z} \gtrsim 0.1$ ),  $\hat{H}_{\text{eff}}$  ceases to be a good approximation. Qualitatively, the same behavior is found for ZnSe (not shown), a smaller value of  $K_c = 0.41 \text{ meV}$  is accounted for by the smaller HH/LH splitting. The value of this constant is a complicated function of system parameters and it can even change sign as shown in Fig. 3(c) where  $K_c = -0.63 \text{ meV}$ . Parameters used in this figure ( $\gamma_1 = 4.0$ ,  $\gamma_2 = 1.5$ , and  $\gamma_3 = 1.6$  and  $h = 20 \text{ meV}$ ) do not strictly correspond to published values of any semiconductor, but they can be viewed as reasonable given the uncertainty in experimental determination of the Luttinger parameters. Dependence of the anisotropy constants for ZnSe and CdTe QDs on  $h$  is summarized in Table II.

Let us now return to noncubic QDs. As already explained, the sizable  $g$ -factor anisotropies shown in Fig. 2(b), relevant to the case of weak magnetism ( $\tilde{Z} \ll 1$ ), translate into an additional term  $AF_1 = K_u n_z^2$  in the free energy of Eq. (2) where  $K_u = -kA$  up to linear order in  $\tilde{Z} \propto k$ . Typically,  $K_u$  exceeds

TABLE II. Magnetic anisotropy constants (in meV) for a  $16 \times 16 \times 16 \text{ nm}^3$  (cubic) and  $16 \times 16 \times 8 \text{ nm}^3$  (deformed) ZnSe and CdTe magnetic QD as a function of exchange splitting (or dimensionless parameter  $\tilde{Z}$  as for CdTe).

$h$ (meV)	$\tilde{Z}$	Cubic		Deformed			
		ZnSe	CdTe	ZnSe		CdTe	
		$K_c$	$K_c$	$K_c$	$K_u$	$K_c$	$K_u$
10	0.55	0.11	0.24	0.23	-3.79	0.35	-3.90
20	1.1	0.20	0.43	0.36	-5.52	0.62	-6.21
30	1.7	0.28	0.59	0.44	-6.29	0.83	-7.59
40	2.2	0.35	0.71	0.50	-6.72	1.01	-8.56
50	2.8	0.41	0.83	0.56	-7.01	1.16	-9.30

$K_c$  already for small QD deformation ( $\lambda$  slightly over one), and the data in Fig. 3(b) imply  $K_u$  almost an order of magnitude larger than  $K_c$  for  $\lambda = 2$  (see also data in Fig. 2 where  $g_z \gg g_x$ ). Regardless of the contributions to  $K_u$  of higher order in  $\tilde{Z}$ , data in Table II imply an out-of-plane easy axis (in the [001] direction) as it is the case in QWs. However, upon deforming of a QD, the easy axis does not abruptly jump from [111] to [001] but smoothly interpolates between these two directions. A similar effect, easy-axis shifting as a function of some system parameter, is also known in bulk DMS [(Ga,Mn)As epilayers in particular; see Fig. 8 in Ref. 15]. Easy axes as a function of QD shape (oblate dots,  $\lambda > 1$ ) and effective exchange splitting  $\tilde{Z}$  are summarized in Fig. 3(d), and the mentioned gradual shift of easy axis is indicated by shading between regions (3) and (2) (easy axes [111] and [001], respectively). On the other hand, the easy-axis position changes abruptly between (1) and (3) or (1) and (2); region (1) corresponds to easy axis in the plane perpendicular to [001] (with anisotropies within this plane being very small). The abrupt changes reflect ground-state crossings, such as the one with  $\lambda$  described below Eq. (14), while the gradual ones stem from level mixing caused by  $\hat{H}_{\text{ex}}$ .

Finally, we comment on MA in QDs occupied by more than one hole. As already mentioned above, one possible approach is to discuss open- and closed-shell systems separately. This notion is based on the concept of the QD being an artificial atom, the levels of which are organized into shells comprising of spin-up and spin-down orbitals. Whenever a shell is completely filled (closed), the numbers of spin-up and spin-down carriers are equal, hence their total spin is zero. If the QD is magnetically doped, no magnetic ordering is expected and also no MA. However, strong SO coupling puts this concept into question since it mixes different shells and also invalidates the spin-up and -down labels of individual orbitals. The MA as a function of particle number  $N_p$  strongly varies, both quantitatively and qualitatively. By comparing the  $N_p = 1$  and 2 cases of a cubic CdTe QD, that is,  $F_0(\mathbf{e}_M) = E_1$  and  $F_0(\mathbf{e}_M) = E_1 + E_2$  of Fig. 3(a), we find that while the easy axis [111] in the former case is relatively “soft” (energy difference between  $\mathbf{e}_M \parallel [111]$  and  $[110]$  is “only”  $\approx 0.1$  meV), the QD with two holes has a “robust” easy axis [110] and the corresponding minimum in  $F_0(\mathbf{e}_M)$  is as deep as 0.3 meV. MA as a function of  $N_p$  displays rich behavior and one can therefore envision control of nanomagnetism by electrostatic gating, illumination (used to photoinduce carriers), and possibly also temperature, known to alter the magnetic ordering in the bulklike structures.<sup>18,40</sup>

#### IV. CONCLUSIONS

We have discussed two approaches to magnetic anisotropies in quantum dots (QDs) described by a generic model in Eq. (1). An effective Hamiltonian for individual Kramers doublets allows us to express the energetics of a magnetically doped QD in terms of only three parameters (anisotropic  $g$  factor) if the exchange splitting due to the magnetic ions is relatively small. On the other hand, if the exchange splitting is large or the QD’s symmetry is too high, the symmetry-based expansion of the magnetocrystalline energy in powers of the direction cosines of magnetization may in principle contain infinitely many terms (each of them quantified by one parameter).

Focusing on manganese-doped semiconductor QDs, we find that only first few magnetocrystalline terms are appreciable, present their values, and show in Fig. 3(d) a diagram of magnetic anisotropies in the QD parameter space. While we consider only a relatively small parameter range in that diagram, and the barriers between individual free-energy minima are relatively low, it demonstrates that the QDs may have rich magnetic anisotropies. In spintronics,<sup>18,19,41</sup> these systems could thus enable confinement-controlled multilevel logic and provide electrical spin injection in lasers with desirable perpendicular anisotropy that could enhance their performance.<sup>42</sup> Our results provide a starting point for further studies of nanoscale magnetism in QDs. Such studies could relax the mean-field approximation, include multiple-carrier states,<sup>22,43</sup> or the effect of strain.

#### ACKNOWLEDGMENTS

This work was supported by DOE-BES DE-SC0004890, NSF-DMR 0907150, AFOSR-DCT FA9550-09-1-0493, US ONR N0000140610123, and NSF-ECCS 1102092.

#### APPENDIX A

The downfolding of  $\hat{H}_{\text{QD}} + \hat{H}_{\text{ex}}$  to  $\hat{H}_{\text{eff}}$  is indeed possible for the two example systems discussed in Secs. II A and II B. To prove this, we first transform the basis  $|K_1\rangle, |K_2\rangle$  to  $|K'_1\rangle, |K'_2\rangle$  where  $\tilde{t}_z$  of Eq. (7) is diagonal and then verify that the diagonal elements of  $\tilde{t}_x$  and  $\tilde{t}_y$  vanish. This procedure has to be applied to each Kramers doublet of interest. In the case of  $\hat{H}_1$  in Eq. (3), this is done simply by construction [e.g.,  $|K'_1\rangle, |K'_2\rangle$  for the upper doublet in Fig. 1(a) is just  $|J_z = 3/2\rangle, |J_z = -3/2\rangle$ ]. In the model described by  $\hat{H}_2$ , one can split the Hilbert space into two disjoint subspaces  $\mathcal{H}_1, \mathcal{H}_2$  and the above assertion can be shown to hold if  $|K'_1\rangle \in \mathcal{H}_1$  and  $|K'_2\rangle \in \mathcal{H}_2$ . (The decomposition  $\mathcal{H} \oplus \mathcal{H}_1$  relies on  $\hat{H}_{\text{ex}}$  being independent of space coordinates; relaxing the mean-field treatment of Mn magnetic moments thus introduces corrections to  $\hat{H}_{\text{eff}}$ .) Finally, one adjusts the relative phase between  $|K'_1\rangle$  and  $|K'_2\rangle$ , so that the matrix  $\tilde{t}_x$  is real and  $\tilde{t}_y$  purely imaginary.

#### APPENDIX B

This appendix explains the relation between the anisotropic  $g$  factors and Eq. (2). The eigenvalues of  $\hat{H}_{\text{eff}}$  are two numbers of equal magnitude and opposite sign, the lower of which is (for  $h > 0$ )

$$-h\sqrt{n_x^2 g_x^2 + n_y^2 g_y^2 + n_z^2 g_z^2}. \quad (\text{B1})$$

Let us consider, for example, a single hole in a cuboid QD of dimensions  $\lambda L \times \lambda L \times L$  (such as it corresponds to data in Table I) so that  $g_x = g_y$ . Expression (B1), which now equals  $F(\mathbf{e}_M)$ , can be rewritten as

$$-\frac{h\sqrt{g_x^2 + g_z^2}}{\sqrt{2}} \sqrt{1 + \frac{g_z^2 - g_x^2}{g_z^2 + g_x^2} (n_z^2 - n_x^2 - n_y^2)} \quad (\text{B2})$$

and developed in terms of a small parameter  $A = (g_z^2 - g_x^2)/(g_z^2 + g_x^2)$ , which quantifies the QD asymmetry as

$$-k(1 - \frac{1}{2}A) - Akn_z^2 + \frac{1}{8}A^2k(2n_z^2 - 1)^2 + \dots, \quad (\text{B3})$$

where  $k = h\sqrt{(g_x^2 + g_z^2)/2}$ . The first term does not depend on the magnetization direction, hence it can be disregarded for the purposes of magnetic anisotropy analysis.

### APPENDIX C

We derive Eq. (14) in this appendix and discuss the details of the model considered in Sec. II B. Energies  $E/\mathcal{E}_0$  in Fig. 2(a) are calculated by numerical diagonalization of  $\hat{H}_2$  with  $h = 0$ , a matrix constructed of  $4 \times 4$  blocks  $\langle m_x m_y m_z | \hat{H}_{\text{KL}} | m'_x m'_y m'_z \rangle / \mathcal{E}_0$  introduced at the beginning of Sec. II B. The basis of  $\hat{H}_{\text{QD}}$  consists thus of direct product states  $|m_x m_y m_z\rangle \otimes |J_z\rangle$  where  $|J_z\rangle$  are the four-spinors of total angular momentum  $J = 3/2$ , which are eigenstates to  $\hat{J}_z$ . For practical purposes, we cut off the basis by  $m_x, m_y, m_z \leq 6$ , resulting in  $\hat{H}_{\text{QD}}$  of dimension 864. Eigenvalues are typically converged to better than 0.1 meV for this cutoff.

The matrix  $\hat{H}_{\text{QD}}/\mathcal{E}_0$  is block diagonal for  $\gamma_2 = \gamma_3 = 0$  and the block  $m_x, m_y, m_z$  has a fourfold-degenerate eigenvalue

$$(m_x/\lambda_x)^2 + (m_y/\lambda_y)^2 + m_z^2. \quad (\text{C1})$$

Dimensionless energies on the left of Fig. 2(a) correspond to  $\lambda_x = \lambda_y = 1$  and are hence integers. The lowest level  $E/\mathcal{E}_0 = 3$  belongs to  $(m_x, m_y, m_z) = (1, 1, 1)$ , while the first excited state  $E/\mathcal{E}_0 = 6$  entails an additional threefold geometric degeneracy corresponding to orbital states  $(1, 1, 2)$ ,  $(1, 2, 1)$ , and

$(2, 1, 1)$ ; the  $E/\mathcal{E}_0 = 6$  level for  $\gamma_2 = \gamma_3 = 0$  is thus twelvefold degenerate.

Next, we can treat the HH-LH splitting as a perturbation when  $\gamma_2$  and  $\gamma_3$  are turned on. In the lowest order, mixing between different  $(m_x, m_y, m_z)$  blocks can be neglected except for the case when their energies were equal at  $\gamma_2 = \gamma_3 = 0$  as in the case of the three blocks of the  $E/\mathcal{E}_0 = 6$  level. With coupling to the remote levels disregarded, we are left with a  $12 \times 12$  matrix in this case, which can be diagonalized analytically. It turns out to have two fourfold-degenerate eigenvalues

$$E_4^\pm/\mathcal{E}_0 = 6 + \frac{64}{3\pi^2} \frac{\gamma_2}{\gamma_1} \left( s \pm \sqrt{s^2 + \frac{81\pi^4}{1024}} \right) \quad (\text{C2})$$

and two twofold-degenerate ones

$$E_2^\pm/\mathcal{E}_0 = 6 - \frac{128}{3\pi^2} \frac{\gamma_2}{\gamma_1} \left( s \mp \frac{9\pi^2}{64} \right). \quad (\text{C3})$$

The lowest of these four energies is  $E_2^-$  and it is shown in Fig. 2(a) for  $s \equiv \gamma_3/\gamma_2 = 1$  as a solid line which crosses the horizontal line  $E/\mathcal{E}_0 = 3$  corresponding to the  $(m_x, m_y, m_z) = (1, 1, 1)$  quadruplet, which does not shift in energy to the first order of this perturbation analysis. Equation (14) is the solution of  $E_2^- = 3\mathcal{E}_0$  for  $\gamma_2/\gamma_1$  under the assumption  $s = 1$ . Such level crossing (as a function of  $\gamma_2/\gamma_1$ ) is genuinely due to the confinement and no level crossings occur in bulk as long as  $0 < \gamma_2/\gamma_1 < 1/2$ .

<sup>1</sup>U. Welp, V. K. Vlasko-Vlasov, X. Liu, J. K. Furdyna, and T. Wojtowicz, *Phys. Rev. Lett.* **90**, 167206 (2003).

<sup>2</sup>X. Liu, Y. Sasaki, and J. K. Furdyna, *Phys. Rev. B* **67**, 205204 (2003).

<sup>3</sup>J. Fernández-Rossier and R. Aguado in *Handbook of Spin Transport and Magnetism*, edited by E. Y. Tsybmal and I. Žutić (CRC Press, New York, 2012).

<sup>4</sup>D. R. Yakovlev and W. Ossau in *Introduction to the Physics of Diluted Magnetic Semiconductors*, edited by J. Kossut and J. A. Gaj (Springer, New York, 2010).

<sup>5</sup>R. Beaulac, L. Schneider, P. I. Archer, G. Bacher, and D. R. Gamelin, *Science* **325**, 973 (2009).

<sup>6</sup>I. R. Sellers, R. Oszwałdowski, V. R. Whiteside, M. Eginligil, A. Petrou, I. Žutić, W.-C. Chou, W. C. Fan, A. G. Petukhov, S. J. Kim, A. N. Cartwright, and B. D. McCombe, *Phys. Rev. B* **82**, 195320 (2010).

<sup>7</sup>F. Henneberger and J. Puls, in *Introduction to the Physics of Diluted Magnetic Semiconductors*, edited by J. Kossut and J. A. Gaj (Springer, New York, 2010).

<sup>8</sup>R. M. Abolfath, A. G. Petukhov, and I. Žutić, *Phys. Rev. Lett.* **101**, 207202 (2008).

<sup>9</sup>A. O. Govorov, *Phys. Rev. B* **72**, 075359 (2005); **72**, 075358 (2005).

<sup>10</sup>D. A. Bussian, S. A. Crooker, Ming Yin, M. Brynda, A. L. Efros, and V. I. Klimov, *Nat. Mater.* **8**, 35 (2009).

<sup>11</sup>R. Oszwałdowski, I. Žutić, and A. G. Petukhov, *Phys. Rev. Lett.* **106**, 177201 (2011).

<sup>12</sup>S. T. Ochsenein, Y. Feng, K. M. Whitaker, E. Badaeva, W. K. Liu, X. Li, and D. R. Gamelin, *Nat. Nanotechnol.* **4**, 681 (2009); I. Žutić and A. G. Petukhov, *ibid.* **4**, 623 (2009).

<sup>13</sup>H. Enaya, Y. G. Semenov, J. M. Zavada, and K. W. Kim, *J. Appl. Phys.* **104**, 084306 (2008).

<sup>14</sup>C. Le Gall, R. S. Kolodka, C. L. Cao, H. Boukari, H. Mariette, J. Fernández-Rossier, and L. Besombes, *Phys. Rev. B* **81**, 245315 (2010).

<sup>15</sup>J. Zemen, J. Kučera, K. Olejník, and T. Jungwirth, *Phys. Rev. B* **80**, 155203 (2009).

<sup>16</sup>L. Dreher, D. Donhauser, J. Daeubler, M. Glunk, C. Rapp, W. Schoch, R. Sauer, and W. Limmer, *Phys. Rev. B* **81**, 245202 (2010).

<sup>17</sup>T. L. Linnik, A. V. Scherbakov, D. R. Yakovlev, X. Liu, J. K. Furdyna, and M. Bayer, *Phys. Rev. B* **84**, 214432 (2011).

<sup>18</sup>I. Žutić, J. Fabian, and S. Das Sarma, *Rev. Mod. Phys.* **76**, 323 (2004).

<sup>19</sup>J. Fabian, A. Matos-Abiague, Ch. Ertler, P. Stano, and I. Žutić, *Acta Phys. Slov.* **57**, 565 (2007).

<sup>20</sup>S. D. Bader, *Rev. Mod. Phys.* **78**, 1 (2006).

<sup>21</sup>J. Fernández-Rossier and R. Aguado, *Phys. Rev. Lett.* **98**, 106805 (2007).

<sup>22</sup>S. J. Cheng, *Phys. Rev. B* **79**, 245301 (2009).

<sup>23</sup>F. V. Kyrychenko and J. Kossut, *Phys. Rev. B* **70**, 205317 (2004).

<sup>24</sup>B. Lee, T. Jungwirth, and A. H. MacDonald, *Phys. Rev. B* **61**, 15606 (2000).

<sup>25</sup>I. A. Merkulov and K. V. Kavokin, *Phys. Rev. B* **52**, 1751 (1995).

<sup>26</sup>C. E. Pryor and M. E. Flatté, *Phys. Rev. Lett.* **96**, 026804 (2006).

<sup>27</sup>A. K. Bhattacharjee, *Phys. Rev. B* **76**, 075305 (2007).

- <sup>28</sup>Magnetostatic shape anisotropy will compete with MAE as soon as the QD is not perfectly cubic. To estimate the shape anisotropy energy, we use parameters similar to those discussed in Sec. III. Taking  $\tilde{Z} = 0.05$  of Eq. (17) and  $\lambda = 1.1$  as a reference point (in-plane magnetization in a  $L = 8$  nm QD is preferred to  $\mathbf{e}_M \parallel \hat{z}$  by  $\sim 0.1$  meV), magnetostatic shape anisotropy (Ref. 15) does not reach even  $1 \mu\text{eV}$ .
- <sup>29</sup>See Sec. III A of Ref. 19 for an introduction to Kramers doublets. Note that multiple doublets may sometimes be degenerate either because of symmetry or by accident.
- <sup>30</sup>L. Besombes, Y. Léger, L. Maingault, D. Ferrand, H. Mariette, and J. Cibert, *Phys. Rev. Lett.* **93**, 207403 (2004); *Phys. Rev. B* **71**, 161307 (2005).
- <sup>31</sup>I. A. Merkulov and A. V. Rodina in *Introduction to the Physics of Diluted Magnetic Semiconductors*, edited by J. Kossut and J. A. Gaj (Springer, New York, 2010).
- <sup>32</sup>A. G. Petukhov, W. R. L. Lambrecht, and B. Segall, *Phys. Rev. B* **53**, 3646 (1996).
- <sup>33</sup>P. S. Dorozhkin, A. V. Chernenko, V. D. Kulakovskii, A. S. Brichkin, A. A. Maksimov, H. Schoemig, G. Bacher, A. Forchel, S. Lee, M. Dobrowolska, and J. K. Furdyna, *Phys. Rev. B* **68**, 195313 (2003).
- <sup>34</sup>G. Katsaros, V. N. Golovach, P. Spathis, N. Ares, M. Stoffel, F. Fournel, O. G. Schmidt, L. I. Glazman, and S. De Franceschi, *Phys. Rev. Lett.* **107**, 246601 (2011).
- <sup>35</sup>C. Le Gall, A. Brunetti, H. Boukari, and L. Besombes, *Phys. Rev. Lett.* **107**, 057401 (2011).
- <sup>36</sup>Material parameters were taken from the following sources. CdTe:  $\gamma_{1,2,3}$  from Ref. 37,  $J_{pd}$  from Ref. 23. ZnSe:  $\gamma_{1,2,3}$  from Ref. 38.
- <sup>37</sup>T. Friedrich, J. Kraus, M. Meininger, G. Schaack, and W. O. G. Schmitt, *J. Phys.: Condens. Matter* **6**, 4307 (1994).
- <sup>38</sup>H. Venghaus, *Phys. Rev. B* **19**, 3071 (1979).
- <sup>39</sup>We basically follow the conventions of Eq. (12) in Ref. 15 with aesthetically more pleasing  $n_x^4 + n_y^4 + n_z^4 = 1 - 2(n_x^2 n_y^2 + n_y^2 n_z^2 + n_z^2 n_x^2)$ .  $K_c$  equals  $B_c$  [Eq. (2) of Ref. 17] or  $B_{x^4} = B_{z^4}$  [Eq. (21) of Ref. 16].
- <sup>40</sup>T. Jungwirth, Jairo Sinova, J. Mašek, J. Kučera, and A. H. MacDonald, *Rev. Mod. Phys.* **78**, 809 (2006); H. Ohno, D. Chiba, F. Matsukura, T. Omiya, E. Abe, T. Dietl, Y. Ohno, and K. Ohtani, *Nature (London)* **408**, 944 (2000); S. Koshihara, A. Oiwa, M. Hirasawa, S. Katsumoto, Y. Iye, C. Urano, H. Takagi, and H. Munekata, *Phys. Rev. Lett.* **78**, 4617 (1997); A. G. Petukhov, I. Žutić, and S. C. Erwin, *ibid.* **99**, 257202 (2007); M. J. Calderón and S. Das Sarma, *Phys. Rev. B* **75**, 235203 (2007); V. Krivoruchko, V. Tarenkov, D. Varyukhin, A. D'yachenko, O. Pashkova, and V. Ivanov, *J. Magn. Magn. Mater.* **322**, 915 (2010); D. Chiba, M. Sawicki, Y. Nishitani, Y. Nakatani, F. Matsukura, and H. Ohno, *Nature* **455**, 515 (2008); E. Dias Cabral, M. A. Boselli, R. Oszwaldowski, I. Žutić, and I. C. da Cunha Lima, *Phys. Rev. B* **84**, 085315 (2011).
- <sup>41</sup>*Concepts in Spin Electronics*, edited by S. Maekawa (Oxford University Press, Oxford, 2006).
- <sup>42</sup>M. Holub, J. Shin, D. Saha, and P. Bhattacharya, *Phys. Rev. Lett.* **98**, 146603 (2007); S. Hövel, N. C. Gerhardt, M. R. Hofmann, F.-Y. Lo, A. Ludwig, D. Reuter, A. D. Wieck, E. Schuster, H. Wende, W. Keune, O. Petravic, and K. Westerholt, *Appl. Phys. Lett.* **93**, 021117 (2008); C. Gøthgen, R. Oszwaldowski, A. Petrou, and I. Žutić, *ibid.* **93**, 042513 (2008); J. Lee, W. Falls, R. Oszwaldowski, and I. Žutić, *ibid.* **97**, 041116 (2010); G. Boéris, J. Lee, K. Výborný, and I. Žutić, *ibid.* **100**, 121111 (2012).
- <sup>43</sup>N. T. T. Nguyen and F. M. Peeters, *Phys. Rev. B* **80**, 115335 (2009); F. Qu and P. Hawrylak, *Phys. Rev. Lett.* **96**, 157201 (2006).